https://doi.org/10.18321/ectj1432

Steam/CO_2 Reforming of Methane Over Impregnated Ni/CeO_2 Catalysts: Effect of Sample Composition on Their Activity and Stability

E.V. Matus[1*], O.B. Sukhova[1], I.Z. Ismagilov[1], V.A. Ushakov[1], S.A. Yashnik[1], M.A. Kerzhentsev[1], Z.R. Ismagilov[1,2]

[1]Boreskov Institute of Catalysis, Siberian Branch, RAS, 5, Ac. Lavrentieva ave., Novosibirsk, Russia
[2]Federal Research Center of Coal and Coal Chemistry, Siberian Branch, RAS, 18, pr. Sovetskiy, Kemerovo, Russia

Article info

Received:
7 February 2022

Received in revised form:
28 March 2022

Accepted:
4 May 2022

Keywords:
Ni catalyst, Ceria, Hydrogen, Syngas Bi-reforming, Methane, Biogas

Abstract

Steam/CO_2 reforming of methane was studied at 600–900 °C, molar ratio CO_2/H_2O 0–2 and contact time 0.04–0.15 s over impregnated Ni/CeO_2 catalysts of various compositions. It has been established that with an increase in the Ni content from 2 to 10 wt.%, both the conversion of reactants (X) and the yield of products (Y) increase in the range X_{CH4} 25→80%, X_{CO2} 35→72%, Y_{H2} 30→80%, Y_{CO} 30→75% (at 750 °C). With a further increase in the nickel content to 15%, the process parameters changed slightly, reaching a plateau. Higher nickel content (10 vs. 2 wt.%) ensures stable operation of the catalyst over time. The functional performance of the catalysts was correlated with physicochemical properties of as-synthesized, activated and spent samples using X-ray fluorescence analysis, low-temperature nitrogen adsorption, X-ray diffraction analysis, electron microscopy, and thermal analysis. It was shown that the Ni content affects the thermal stability, the textural, structural and redox characteristics of the samples. The 10% Ni/CeO_2 catalyst was chosen as the optimal one due to higher H_2 productivity, and sufficient resistance to sintering and coking. This sample provides a stable hydrogen yield of 85% in steam/CO_2 reforming of methane at 800 °C, CO_2/H_2O = 2 and a contact time 0.15 s.

1. Introduction

Synthesis gas (or syngas) is a crucial intermediate for the production of valuable compounds on an industrial scale, such as hydrogen, methanol, liquid fuels and other chemical products [1]. It is a mixture of hydrogen and carbon monoxide whose H_2/CO molar ratio can be adjusted by varying the raw materials used and the production technology. Synthesis gas can be obtained from oil, natural gas and coal. Natural gas is a traditional feedstock for the production of synthesis gas by steam reforming (1), dry reforming (2) and partial oxidation (3) of methane, or a combination of these processes – steam-CO_2 reforming (4), autothermal reforming (5), tri-reforming (6) of methane. The combination of traditional conversion methods makes it possible to increase the energy efficiency of the technology and ensure the production of synthesis gas suitable in composition for subsequent use. Biogas formed during biomass or organic waste conversion serves as an alternative feedstock for the production of synthesis gas [2]. Biogas composition depends on the type of feedstock. It can contain CH_4 (50–80 vol.%), CO_2 (20–55 vol.%), water and other components in small quantities (CO, H_2, H_2S, N_2) suitable for its reforming into a hydrogen-containing gas [3, 4]. An important task today is the creation of catalysts that provide high and stable conversion of a methane-containing gas of variable composition.

Extensive information on methane reforming catalytic systems is presented in recent reviews [5–12]. Supported Ni catalysts are usually used as catalysts for the methane reforming process: Ni/CeO_2 [13, 14], Ni/SiC [15], Ni-MgO-(Ce,Zr)O_2 [16], Ni-Zn-Mg-Al [17], Ni@MWCNT/Ce [18], Ni/$CeZrO_2$/$MgAl_2O_4$ [19], Ni@SiO_2 [20], Ni/Al_2O_3 [21]. Nickel content varies over a wide range – from 1 to 30 wt.%. Its optimal content

*Corresponding author.
E-mail addresses: matus@catalysis.ru

$$CH_4 + H_2O \leftrightarrow CO + 3H_2 \quad \Delta_rH^o_{298} = 206 \text{ kJ/mol} \quad (1)$$

$$CH_4 + CO_2 \leftrightarrow 2CO + 2H_2 \quad \Delta_rH^o_{298} = 247 \text{ kJ/mol} \quad (2)$$

$$CH_4 + 0.5O_2 \rightarrow CO + 2H_2 \quad \Delta_rH^o_{298} = -36 \text{ kJ/mol} \quad (3)$$

$$2CH_4 + CO_2 + H_2O \rightarrow 3CO + 5H_2 \quad \Delta_rH^o_{298} = 227 \text{ kJ/mol} \quad (4)$$

$$2CH_4 + 0.5O_2 + H_2O \rightarrow 2CO + 5H_2 \quad \Delta_rH^o_{298} = 85 \text{ kJ/mol} \quad (5)$$

$$3CH_4 + 0.5O_2 + H_2O + CO_2 \rightarrow 4CO + 7H_2 \quad \Delta_rH^o_{298} = 139 \text{ kJ/mol} \quad (6)$$

depends on the composition of the catalyst and the process conditions. In general, the dependence of the activity on the nickel content is non-linear, since at low Ni contents, catalyst deactivation is observed due to sintering of the active component, and in the case of high contents, due to coking [17]. Work is underway to improve the formula and method of preparing catalysts to increase their resistance to sintering, oxidation and the formation of carbon deposits. The influence of the precursor type [15, 22] and the content of the active component [13, 17, 23, 24], the composition of the support [10, 16, 19, 25–28], and the method of preparation of the catalyst [16, 21, 29, 30] on its activity and operation stability in methane reforming was revealed. An improvement in the functional properties of Ni/SiC was noted when using nickel nitrate or acetate instead of chloride or citrate as precursors [15]. Among the effective approaches for obtaining deactivation-resistant Ni catalysts, one can single out the stabilization of highly dispersed nickel particles due to the implementation of strong metal–support interaction [15, 31–34], support modification [19, 35–37], or promotion of the active component [38–40].

Nickel-cerium catalysts have a high potential in methane reforming processes due to the extended nickel-cerium interface with specific active sites, the basic and redox properties of cerium oxide, which can activate oxygen, water and CO_2 and help to eliminate carbon deposits [26, 41–44]. It was shown that small Ni clusters at CeO_2 step edges are highly active in DRM (dry reforming of methane) due to deep interaction with support and realization of specific electronic Ni state [43]. To stabilize such species in the oxide matrix, a low nickel content is preferred. The direct correlation between the initial methane conversion and the fraction of accessible Ni also illustrates the advantage of the finely dispersed state of nickel [45]. In addition, fine nickel particles (< 10 nm) are more resistant to coking [14]. However, the high initial dispersion of Ni is not always a guarantee of the operation stability of the catalyst [41, 45]. For example, during DRM over low–loaded Ni/CeO_2 catalyst (0.8 wt.% Ni) CH_4 conversion dropped from 71 to 35% after 8 h time on stream [41]. According to [45], by improving the dispersion of Ni to isolated cations, the Ni particle growth mechanism switches from crystal migration to atomic migration, which leads to higher particle growth rates. Thus, despite the increased interest in the Ni/CeO_2 system and its comprehensive study, the question of the optimal content and particles size of Ni in methane reforming catalysts remains debatable and requires further research.

In this work, for studying the impact of the Ni content on the catalytic activity and stability in steam-CO_2 reforming of methane, impregnated Ni/CeO_2 samples of various compositions were prepared and characterized by X-ray fluorescence analysis, low-temperature nitrogen adsorption, X-ray diffraction analysis, electron microscopy, and thermal analysis. To estimate their ability to convert the feedstock of variable composition into hydrogen-containing gas the testing of Ni/CeO_2 catalysts was carried out in different reaction conditions (600–900 °C, molar ratio CO_2/H_2O 0–2 and contact time 0.04–0.15 s).

2. Experimental

2.1. Catalyst preparation

Ni/CeO_2 catalysts of different compositions were prepared by the incipient wetness impregnation method. For this, the required amount of an aqueous solution of nickel nitrate hexahydrate $Ni(NO_3)_2 \cdot 6H_2O$ of a given concentration was added to the CeO_2 support. The CeO_2 support was prepared by the polymerizable complex method [46]. Then, Ni/CeO_2 samples were dried at 80 °C for 6 h and calcined at 500 °C for 4 h in air. The samples were designated as 2% Ni, 5% Ni, 10% Ni and 15% Ni where the numbers corresponded to the nominal nickel content. X-ray fluorescence analysis showed that the actual content of Ni for 2% Ni (2.2 wt.%), 5% Ni (5.1 wt.%), 10% Ni (11.0 wt.%) and 15% Ni (15.5 wt.%) samples are in good agreement with the calculated Ni content.

2.2. Characterization of catalysts

The Ni/CeO_2 catalysts have been studied by a set of methods: X-ray fluorescence analysis, low-temperature nitrogen adsorption, X-ray diffraction analysis (XRD), electron microscopy, and thermal analysis (TA). A description of the instruments and conditions for the study of catalysts by physicochemical methods can be found in our earlier publications [47, 48].

2.3. Catalytic activity tests

The steam/CO_2 reforming of methane was studied in a flow quartz reactor (internal diameter 11 mm), at atmospheric pressure, temperature 600–850 °C, molar ratio CO_2/H_2O 0–2 and contact time 0.04–0.15 s. Unless otherwise noted, the molar ratio CH_4:CO_2:H_2O:He was 1.0/0.81/0.38/2.8, contact time 0.15 s. The composition of the reaction mixture was analyzed by gas chromatographic analysis using a Kristall 2000M chromatograph. The separation of H_2, He, CO, CO_2, CH_4 was carried out on a steel packed column 2 m long, 3 mm in diameter with SKT carbon (thermal conductivity detector, carrier gas – Ar, 30 cm^3/min, temperature 130 °C). Before the catalytic activity test, the catalyst (0.5 g, fraction 0.25–0.50 mm) was reduced at 800 °C for 1 h in a H_2/He flow with a mixture feed rate of 130 cm^3/min. The activity of the catalysts in the steam/CO_2 reforming of methane was characterized by the total conversion of methane (X_{CH4}), the total conversion of carbon dioxide (X_{CO2}), the yield of hydrogen (Y_{H2}) and the yield of carbon monoxide (Y_{CO}) [49].

The thermodynamic equilibrium analysis was carried out by using the Gibbs free energy minimization method. The program IVTANTHERMO was used.

3. Results and discussion

Figure 1 shows temperature dependences of product concentrations in steam/CO_2 reforming of methane over Ni catalysts of different compositions. In the case of the 2% Ni catalyst (Fig. 1a), the CH_4 and CO_2 conversion starts at 600 °C, but the quantity of reforming products – CO and H_2 are negligible (< 5 vol.%). As the temperature rises, the concentrations of methane and carbon dioxide decrease, while those of CO and hydrogen increase. This tendency is more pronounced for the 10% Ni catalyst (Fig. 1b), for which higher values of H_2 and CO concentrations are achieved in the whole temperature range 600–850 °C. In the presence of a 10% Ni catalyst, the process parameters at 850 °C are close to thermodynamic equilibrium results (Fig. 1c).

The parameters of steam–CO_2 reforming of methane over Ni catalysts depend on their composition (Table 1, Fig. 2a). It was found that with an increase in Ni content from 2 to 10 wt.%, both the conversion of reactants and the yield of products

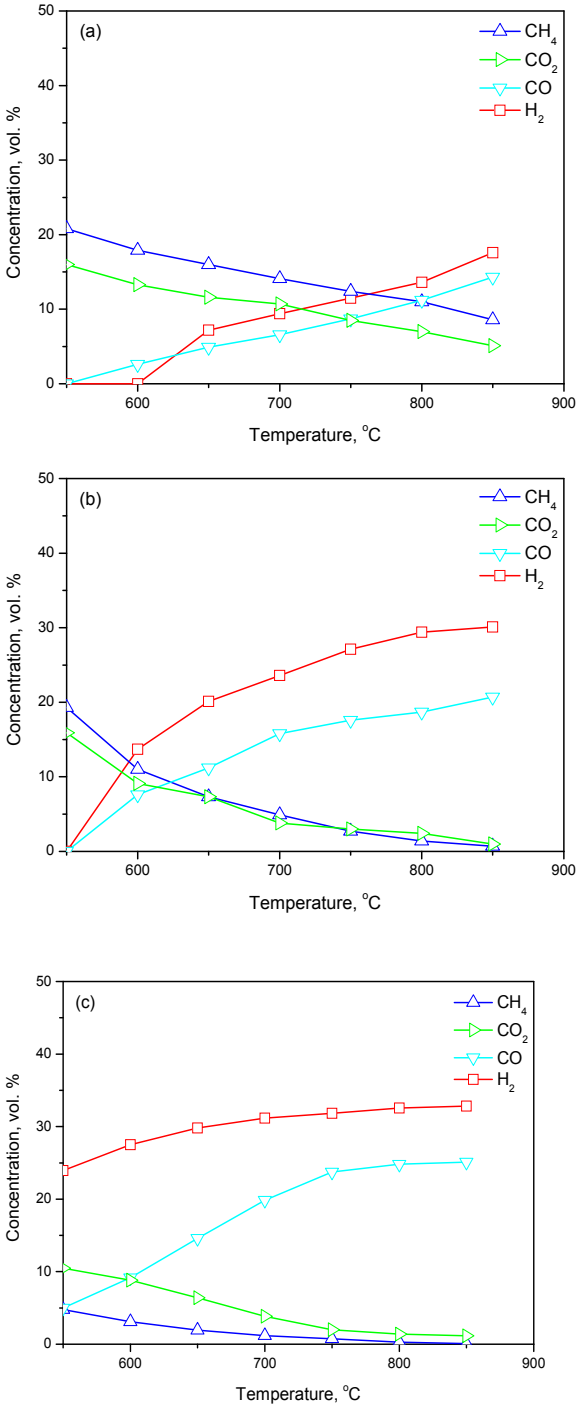

Fig. 1. Temperature dependence of product concentrations in steam/CO_2 reforming of methane over 2% Ni (a) and 10% Ni (b) catalysts, and the thermodynamic equilibrium values (c).

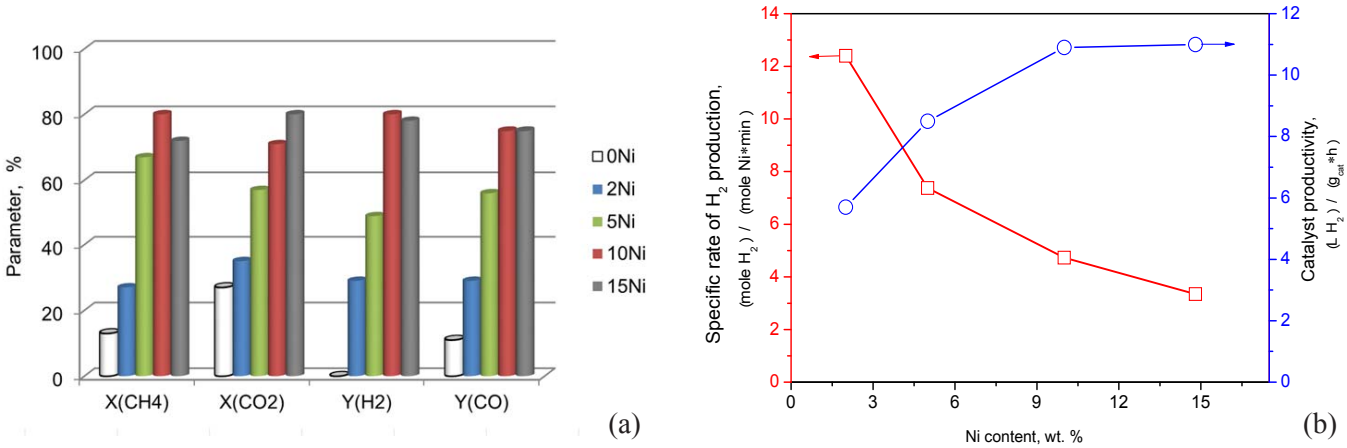

Fig. 2. Effect of Ni content on the parameters of steam – CO_2 reforming of methane at 750 °C (a) and specific rate of H_2 production and catalyst productivity at 850 °C (b) over Ni/CeO_2 catalysts.

increased, reaching the following values at 750 °C: X_{CH4} 25→80%, X_{CO2} 35→72%, Y_{H2} 30→80%, Y_{CO} 30→75%. Catalyst productivity also grew from 5.7 to 11.0 $L_{H2}/(g_{cat}·h)$. The molar ratio CO/H_2 increases noticeably (1.2 vs. 1.5, Table 1). With a further increase in the nickel content to 15%, the process parameters changed slightly, reaching a plateau (Table 1). According to the efficiency of H_2 formation per mole of Ni, the catalysts are arranged in a row 15% Ni < 10% Ni < 5% Ni < 2% Ni, providing at 850 °C, respectively, the specific rate of hydrogen formation 3.4, 4.7, 7.4 and 12.4 $mole_{H2}/(mole_{Ni}·min)$ (Fig. 2b). It can be seen that, in contrast to the conversion and yield indicators, the specific indicator (calculated per mole of the Ni active component) of the catalyst activity decreases with an increase in the nickel content. This may be due to a decrease in the dispersion of the Ni active component and, accordingly, the fraction of available surface active sites.

Increasing contact time from 0.04 to 0.15 sec results in improved process performance: X_{CH4} 30→80%, X_{CO2} 35→70%, Y_{H2} 35→80%, Y_{CO} 35→75% at 750 °C over 10% Ni/CeO_2 catalyst.

Note that the catalysts ensure high methane conversion and the yield of the product in a wide

Table 1
The parameters of steam–CO_2 reforming of methane over Ni/CeO_2 catalysts

Sample	T, °C	X_{CH4}, %	X_{CO2}, %	Y_{H2}, %	Y_{CO}, %	H_2/CO
2% Ni	600	14	17	0	7	0
	700	19	20	23	21	1.4
	800	33	45	35	39	1.2
	850	44	57	48	52	1.2
5% Ni	600	27	9	27	20	1.8
	700	54	45	47	44	1.4
	800	77	69	66	67	1.3
	850	86	75	73	74	1.3
10% Ni	600	29	24	34	27	1.8
	700	65	66	65	63	1.5
	800	89	76	89	82	1.6
	850	95	90	91	90	1.5
15% Ni	600	27	16	41	25	2.2
	700	55	61	61	58	1.4
	800	86	90	90	87	1.4
	850	93	100	96	92	1.4

range of compositions of the initial gaseous medium (Fig. 3). This allows them to operate with a variable composition of the feedstock, for example, biogas.

When the varying concentration of CH_4 and CO_2 in the reaction feed at a fixed molar ratio C/O equal to 0.9, a change in the values of both the conversion of the reagents and the yield of the target reaction products is observed (Fig. 3). With an increase in the molar ratio of CO_2/H_2O in the reaction mixture from 0 to 2, an increase in the conversion of carbon dioxide and the yield of CO, as well as a slight increase in the yield of hydrogen, is observed. The behavior of the dependence of the methane conversion on the CO_2/H_2O ratio depends on the reaction temperature. With an increase in CO_2/H_2O from 0.5 to 2, the conversion of methane in the low-temperature region of the reaction decreases, at T = 800 °C it is the same, and at T = 850 °C, on the contrary, it slightly increases. The H_2/CO value decreases from 4.1 to 0.9 with increasing CO_2/H_2O. It should be noted that the

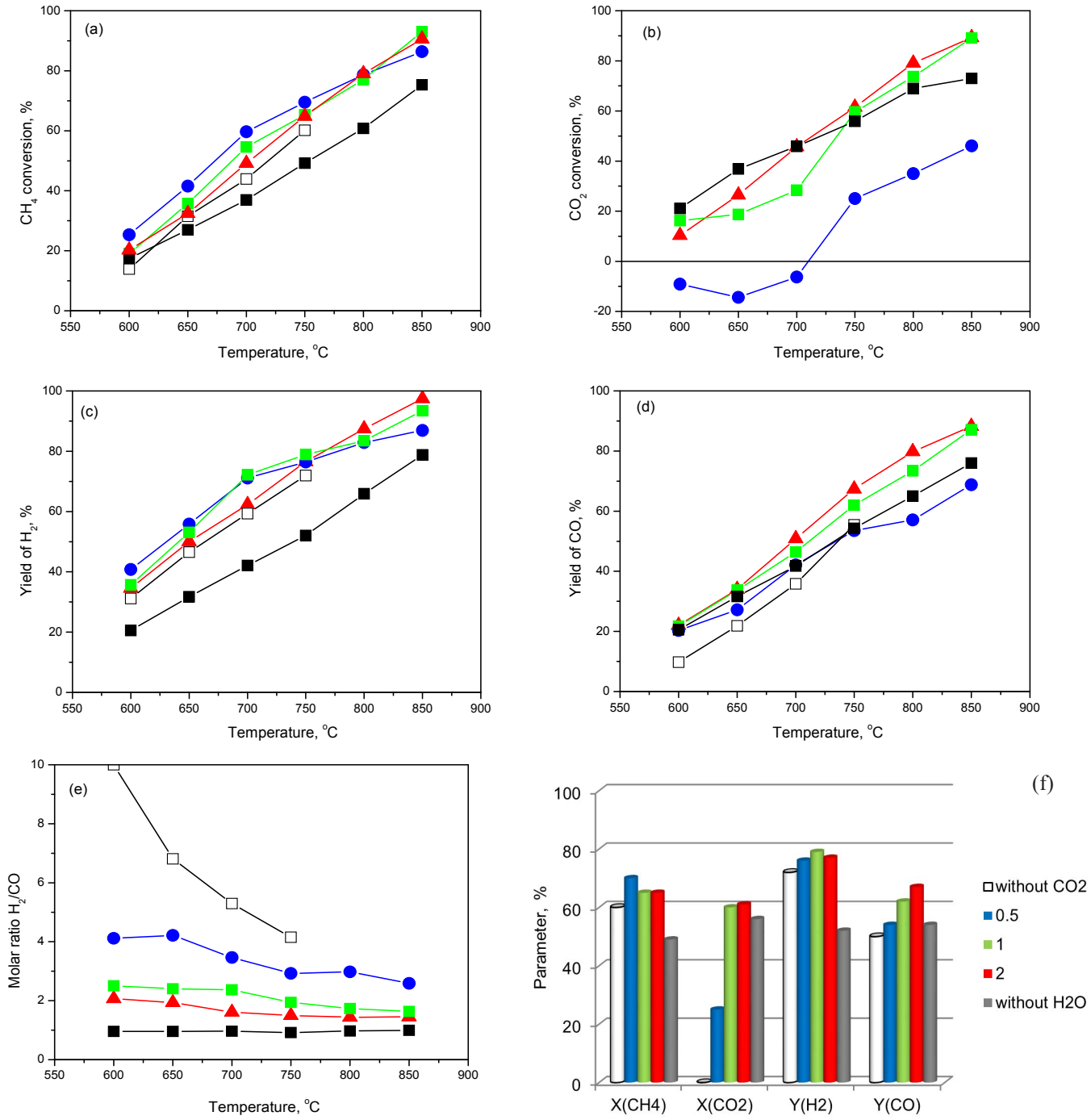

Fig. 3. The steam–CO_2 reforming of methane over 10% Ni/CeO_2 catalyst: effect of the composition of the reaction mixture. Molar ratio CO_2/H_2O: —□— without CO_2; —●— 0.5; —▲— 1; —■— 2; —■— without H_2O.

features of the experiments, where only water served as an oxygen source, were high values of the H_2/CO molar ratio and the formation of a significant amount of carbonaceous deposits. This led to an increase in gas-dynamic resistance and forced the termination of the experiment. The use of only CO_2 as an oxidizing agent (experiments without water) leads to a deterioration in the process parameters (Fig. 3). By modulating the molar ratio of CO_2/H_2O in the feed, the ratio of H_2/CO can be easily adjusted to the desired value within the range of 1–3, which is suitable for further use. The optimal value of the CO_2/H_2O molar ratio can be considered the in range of values 1–2, for which high values of both methane and carbon dioxide conversion are observed, and a high hydrogen yield is also achieved.

Long-term tests of catalysts have shown their satisfactory stability (Fig. 4). Parameters decrease most rapidly in the first hours of the reaction, and then they are stabilized. For the 10% Ni/CeO_2 catalyst for 24 h of testing, the decrease in process parameters was no more than 15%, and for 2% Ni, ~ 40%. Higher values of CO_2 conversion compared to CH_4 conversion in the presence of 2% Ni, in contrast to 10% Ni, where they are comparable, may indicate a significant contribution of the support to CO_2 activation at a low content of the Ni component.

To elucidate the correlation between the functional performance of the catalysts and their physicochemical properties the as-synthesized, activated and spent samples were studied by low-temperature nitrogen adsorption, XRD analysis, electron microscopy, and TA (Table 2, Figs. 5–7).

According to low-temperature nitrogen adsorption data, the as-synthesized samples are mesoporous materials with an average pore diameter of ~10 nm (Table 2). The specific surface area of the catalysts decreases from 85 to 65 m^2/g with an increase in the Ni content from 2 to 15 wt.%, which is due to the blocking of fine pores of the CeO_2 support by the crystallites of the active component phase. The specific surface area of the studied catalysts is lower than those obtained by the Pechini method [48], but it is comparable to that of impregnated samples [15, 42, 50] and is higher than S_{BET} of samples prepared by co-precipitation or combustion synthesis [45]. High-temperature treatment of catalysts in H_2 during activation leads to a significant decrease in their S_{BET} as a result of the transfer NiO to Ni and intensification of sintering processes. Note that the initial differences in textural characteristics level out and the activated samples have S_{BET} of ~4 m^2/g. Under reaction conditions (high temperatures, presence of water vapor), the texture characteristics are not practically changed. Regardless of the Ni content, the S_{BET} of the spent samples is also ~4 m^2/g.

XRD data (Tables 2 and 3) and electron microscopy study (Fig. 5) indicate that CeO_2 and NiO are the main phases in the as-synthesized samples. After calcination at 300–500 °C the average crystallite size of CeO_2 does not change with variation in Ni content. The same average crystallites size for CeO_2 (11 nm) is obtained at high (15 wt.%) and low (2 wt.%) loading of Ni. Conversely, the NiO particle size increases from 3–5 to 50 nm with an increase in the Ni content from 2 to 15 wt.%. In comparison to other supports, such as Al_2O_3, MgO or La_2O_3, CeO_2 provides lower NiO dispersion [32, 51]. It is known that in the case of Al_2O_3, MgO or La_2O_3 oxides, the strong metal-support interaction is realized up to the formation of joint phases after high-temperature calcination.

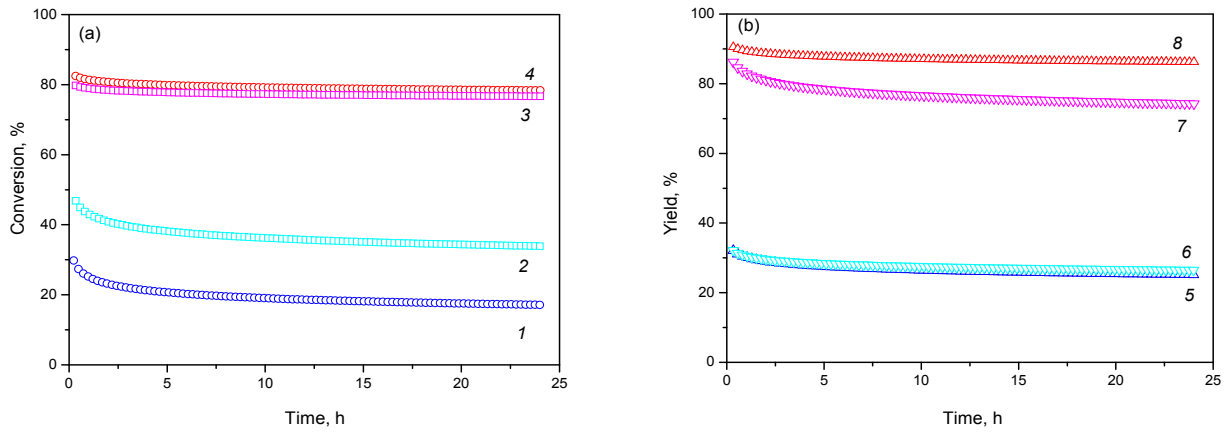

Fig. 4. Conversion of CH_4 (a, curves 1, 4), conversion of CO_2 (a, curves 2, 3), yield of H_2 (b, curves 5, 8) and yield of CO (b, curves 6, 7) in the steam–CO_2 reforming of methane with time on stream at 800 °C over 2% Ni/CeO_2 (curves 1, 2, 5, 6) and 10% Ni/CeO_2 (curves 3, 4, 7, 8).

For CeO_2+NiO system it is not typical and special preparation methods are required for formation of Ce-Ni-O solid solution [44, 48, 52–54]. Although a small part of the nickel cations can exist within the cerium dioxide lattice, forming a surface solid solution and causing an increase in oxygen vacancies [42, 52].

An increase in the calcination temperature of the samples leads to a decrease in the dispersion of the phases due to sintering (Table 3). It can be seen that the nickel content has an effect on the resistance to sintering of the CeO_2 support phase, which resembles the process of inhibition of crystallite growth in the presence of a dopant [45, 55]. In particular, after calcination in air at 700 °C, the average particle size of cerium dioxide is equal to 30, 18, and 14 nm for the CeO_2, 2% Ni, and 5% Ni samples, respectively.

(a)

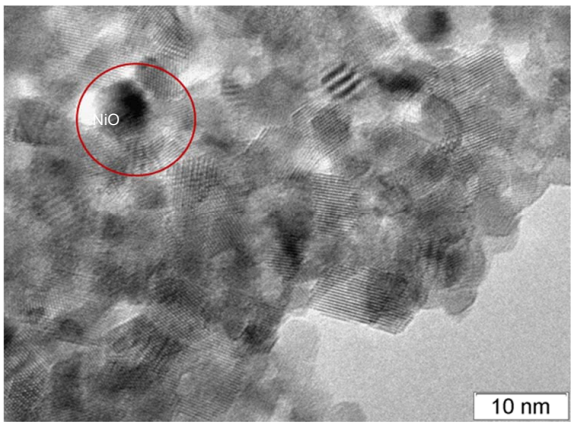

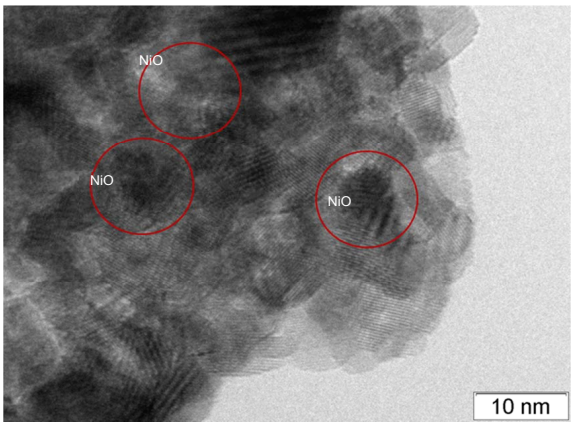

(b)

Fig. 5. Transmission electron microscopy images of as-synthesized 2% Ni/CeO_2 (a) and 10% Ni/CeO_2 (b, [48]) catalysts.

Table 2

Textural and structural properties of as-synthesized, activated and spent Ni/CeO_2 catalysts

Sample	Conditions of treatment*	Textural properties**			XRD data***		Coke content, formed during reaction, wt.%
		S_{BET}, m^2/g	V_{pore}, cm^3/g	D_{pore}, nm	Phase	CSR, nm	
2% Ni	500 °C, air	85	0.22	9.9	CeO_2 (0.5411)	11	-
	800 °C, H_2	4.2	0.05	49.7	CeO_2 (0.5420)	25	-
	800 °C, reaction	4.3	0.04	36.0	CeO_2 (0.5422) Ni	25 50	0.05
5% Ni	500 °C, air	80	0.19	9.6	CeO_2 (0.5411) NiO	11 20	-
	800 °C, H_2	3.9	0.05	51.6	CeO_2 (0.5420) Ni	25 25	-
10% Ni	500 °C, air	75	0.19	10.1	CeO_2 (0.5411) NiO	11 25	-
	800 °C, H_2	4.4	0.05	46.6	CeO_2 (0.5420) Ni	25 25	-
	800 °C, reaction	4.0	0.01	43.0	CeO_2 (0.5417) Ni	25 50	0.1
15% Ni	500 °C, air	65	0.16	9.7	CeO_2 (0.5411) NiO	11 50	-
	800 °C, H_2	4.4	0.08	74.8	CeO_2 (0.5416) Ni	25 25	-

* – as-synthesized (500 °C, air, 4 h), activated (800 °C, H_2, 1 h) and spent (800 °C, reaction, 24 h) samples.
** – the specific surface area (S_{BET}), total pore volume (V_{pore}) and average pore diameter (D_{pore}).
*** – cell parameters (nm, ±0.0003) are indicated in brackets. CSR – the coherent scattering region.

Table 3
Sintering resistance depending on material composition

Sample	The phase composition of samples calcined in air at a different temperatures		
	300 °C	700 °C	900 °C
CeO_2	CeO_2* (9.0)**	CeO_2 (30.0)	CeO_2 (50.0)
2% Ni	CeO_2 (11.0)	CeO_2 (18.5)	CeO_2 (50.0)
5% Ni	CeO_2 (11.0) NiO (15.0)	CeO_2 (14.0) NiO (20.0)	CeO_2 (50.0) NiO (50.0)
10% Ni	CeO_2 (11.0) NiO (15.0)	CeO_2 (14.0) NiO (25.0)	CeO_2 (50.0) NiO (50.0)
15% Ni	CeO_2 (11.0) NiO (50.0)	CeO_2 (14.0) NiO (50.0)	CeO_2 (50.0) NiO (50.0)

* – for the CeO_2 phase, the cell parameter is the same for all samples and equal to 0.5411 nm.
** – for the CeO_2 phase and the NiO phase, the CSR size (nm) is indicated in brackets.

It is known that Ni/CeO_2 system becomes active when Ni^{2+} is reduced to Ni^0 which is accompanied by the transformation of a part of Ce^{4+} to Ce^{3+} [56]. So, before reaction catalysts were reduced. As a result of such activation, the Ni^0 phase is formed with an average particle size of 25 nm (Table 2). This phase becomes less dispersed as a result of sintering under the reaction conditions that are typical for Ni catalysts [45]. It is possible to improve the dispersion of Ni^0 by doping CeO_2 by La or Mg or by using the exsolution approach for catalyst preparation [57, 58]. The CeO_2 phase of the support is retained after activation and reaction, but the average size of its crystallites increases from 11 to 25 nm as well as cell parameters. An increase in the cell parameter (0.5411 → 0.5420 nm) as a result of partial reduction of CeO_2 occurs due to the formation of oxygen vacancies and an increase in the proportion of Ce^{3+} cations, which have a larger cation radius than Ce^{4+} (0.114 vs. 0.097 nm) [59]. The formation of Ni^0 phase occurs in the temperature range of 300–500 °C as is indicated by thermal analysis of samples in a H_2/He flow simulating the process of catalyst activation before the reaction (Fig. 6). According to TPR-H_2 data [48], the reducibility of catalysts increases with increasing Ni content and equals 0.38, 0.58, 1.06 and 0.98, $mole_{H2}/mole_{Ni}$ for 2% Ni, 5% Ni, 10% Ni and 15% Ni samples consequently.

The study of spent catalysts by thermal analysis shows that an insignificant weight loss (~0.25 wt.%) occurs in the low-temperature region (T < 200 °C) due to desorption of water and volatile intermediate products (Fig. 7). Further, at a temperature of 300–500 °C, the weight of the sample increases, which is associated with the oxidation of the Ni^0 active component. The process is accompanied by an exothermic effect, which has a maximum at 400 °C. Weight loss in the region of 500–800 °C is insignificant and amounts to less than 0.1 wt.% and can be assigned to the oxidation of carbonaceous deposits. Higher weight values due to phase transformations and burnout of carbon deposits are observed for a sample with a higher content of the active component. An estimate of the specific rate of formation of carbonaceous deposits at 800 °C showed that it was significantly lower than the specific rate of H_2 formation: $3.2 \cdot 10^{-5}$ $mole_C/(mole_{Ni} \cdot min)$ vs. 4.7 $mole_{H2}/(mole_{Ni} \cdot min)$ for 10% Ni sample. The main pathways of carbon formation are cracking ($CH_4 \rightarrow C + H_2$) and Boudouard reaction ($2CO \rightarrow C + CO_2$). According to thermodynamic data, the selectivity of coke formation in bi-reforming of methane is highly limited at temperatures above 700 °C [49, 60].

Thus, the as-synthesized Ni/CeO_2 catalysts with different Ni content differ by textural, structural and redox properties. With an increase in the nickel content, the specific surface area and the dispersion of the active component decrease, while the reducibility of the catalyst and the resistance to sintering of the support phase CeO_2 improve. The activated samples or the samples after the reaction, on the contrary, are characterized by close values of the S_{BET} and the same phase composition, regardless of the nickel content. So, the

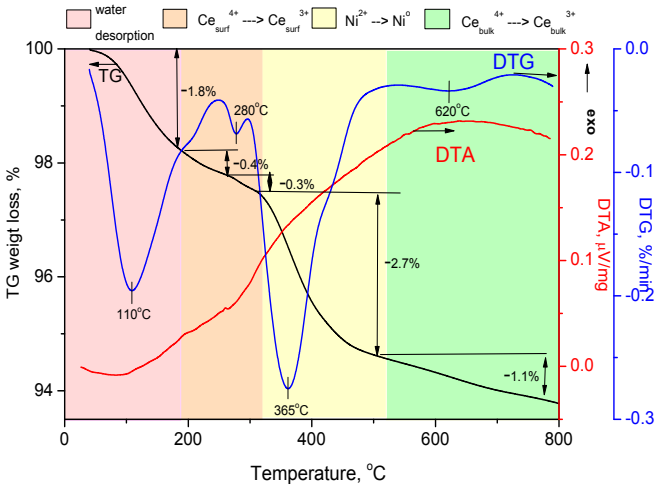

Fig. 6. Thermal analysis of a 10% Ni/CeO_2 sample in a H_2/He flow, simulating the process of catalyst activation before the reaction.

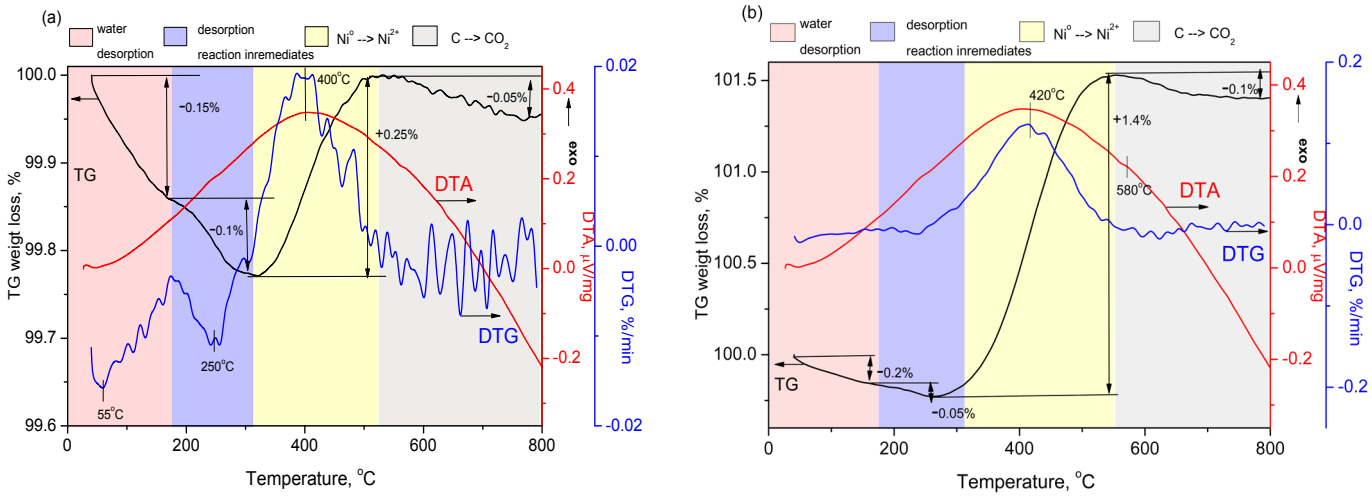

Fig. 7. Thermal analysis of the spent 2% Ni/CeO_2 (a) and 10% Ni/CeO_2 samples (b) (after 24 h on stream) in an air flow.

high activation temperature and subsequent harsh reaction conditions smoothed out the initial textural and structural differences between the samples. Nevertheless, higher H_2 productivity (Fig. 2b) and resistance to deactivation under reaction conditions (Fig. 4) were observed for 10% Ni sample compared to 2% Ni. In situ XAS spectroscopy indicates [61] that under reducing conditions the size and morphology of Ni particles change, which become flattened and strongly stabilized on the partially reduced CeO_2 surface that promoting their stability under reaction. Taking into account the low content of carbonaceous deposits for both our catalysts, the decrease in activity in the initial period of the reaction before reaching a steady state conversion seems to be mainly associated with phase sintering and a decrease in the number of available active sites. By improving the dispersion of Ni to isolated cations in as-synthesized samples, the Ni particle growth mechanism switches from crystal migration to atomic migration, which leads to higher particle growth rates [45]. So the sintering process is more pronounced for low-loaded catalysts, which have higher initial nickel dispersion. Indeed, for cubic or spherical metal particles, the surface atoms/bulk atoms ratio rapidly decreases with increasing particle size [62]. For example, at a particle size of 3 nm, 50% of atoms or ions are on the surface while at a size of 10 nm – ~ 15% and at a size of 25 nm – ~ 5%. Thus, it can be assumed that the differences in the catalytic activity and stability of 2- and 10% Ni catalysts are mainly associated with differences in the mechanism of the growth of Ni particles and the concentration of available Ni^o active sites under reaction conditions. Doping of CeO_2 hinders Ni and CeO_2 sintering and improves process performance [63].

Our 10% Ni catalyst provides high and stable conversion of reagents and high hydrogen yield (at 800 °C X_{CH4} = 80%, Y_{H2} = 85%) that is comparable to or better than literature data for combined steam-CO_2 reforming of methane [64–69]. Namely, in bi-reforming of methane at 800 °C over impregnated Ni/CeO_2 catalyst X_{CH4} is equal to 50% [64], at 800 °C over co-precipitated Ni/CeO_2 – 80% [64], at 900 °C over $Ni–Ce–Fe/Al_2O_3$ – 90% [65], at 800 °C over Ni/SBA-15 – 70% [66], at 800 °C over $Ni/MgAl_2O_4$ – 90% [67], at 800 °C over $Ni/Ce_{0.6}Zr_{0.4}O_2$ – 60% [68], at 700 °C over Ni/ZrO_2 – 45–70% depending on the type of ZrO_2. A significant advantage of the developed Ni/CeO_2 catalysts is their high resistance to coking even at a low steam/CO_2 molar ratio (H_2O/CO_2 = 0.5) used in the initial reaction mixture. In particular, after 24 h on stream 10% Ni sample contains 0.1 wt.% of carbon which corresponds to the carbon accumulation rate of 0.04 $mgC \cdot h^{-1} \cdot g_{cat}^{-1}$ ($3.2 \cdot 10^{-5}$ $mole_C/(mole_{Ni} \cdot min)$). For example, after bi-reforming of methane, 12% Ni/Al_2O_3 catalyst includes 50 wt.% carbonaceous deposits (C) [65], 12% Ni–5% Ce–5% Fe/Al_2O_3 – 2 wt.% of C [65], 5% $Ni/MgAl_2O_4$ – 3 wt.% of C [67], 10% Ni/SBA-15 – 6.4 and 3% B-10% Ni/SBA-15 – 1.5 wt.% of C [66], for 10% Ni/ZrO_2 content of C varies from 0.2 to 47.9 wt.% for different types of ZrO_2 support [69]. This stability of the catalyst to coking may be due to several factors. Firstly, this is connected with the anticoking properties of cerium dioxide support [7, 70]. And secondly, the large size of Ni crystallites, on which, as was shown in [14], the coking rate is lower than for nickel particles with a size of 20–30 nm.

4. Conclusions

In order to obtain a more complete understanding of the design and application of Ni-loaded CeO_2 catalysts, the influence of the composition of Ni/CeO_2 catalysts on their activity, stability and anti-coking properties in steam/CO_2 reforming of methane were studied. The relationship between the performance of catalysts in reaction and their textural, structural and redox properties was established. For as-synthesized Ni/CeO_2 with an increase in the Ni content, the specific surface area of the catalyst and the dispersion of the active component decrease, while the reducibility of the samples and their resistance to sintering improve. The high activation temperature and subsequent harsh reaction conditions smoothed out the initial textural and structural differences between the samples. Nevertheless, compared to 2% Ni, 10% Ni catalyst is characterized, firstly, by higher hydrogen productivity, which means a higher hydrogen concentration in the mixture of reaction products and, secondly, lower deactivation rates. It can be assumed that these differences are mainly associated with differences in the sintering mechanism and the concentration of available Ni^o active sites under reaction conditions. So, the 10% Ni/CeO_2 catalyst was chosen as the optimal one due to its ability to provide high and stable conversion of CH_4 and CO_2 to synthesis gas, high H_2 productivity, efficient operation with various feedstock compositions, resistance to the formation of carbon deposits and low deactivation rate.

Funding

This work was supported by the Ministry of Science and Higher Education of the Russian Federation within the governmental order for Boreskov Institute of Catalysis (project AAAA-A21-121011490008-3).

The authors are grateful to A.A. Pochtar, A.A. Leonova and Dr. E.Yu. Gerasimov for their assistance with catalyst characterization.

References

[1]. J. van de Loosdrecht, J.W. (Hans) Niemantsverdriet. 5.4 Synthesis Gas to Hydrogen, Methanol, and Synthetic Fuels, in: Chemical Energy Storage, 2012, pp. 443–458. DOI: 10.1515/9783110266320.443

[2]. G. Glivin, N. Kalaiselvan, V. Mariappan, M. Premalatha, P.C. Murugan, J. Sekhar, *Fuel* 302 (2021) 121153. DOI: 10.1016/j.fuel.2021.121153

[3]. R. Salehi, S. Chaiprapat, *Environ. Eng. Res.* 27 (2021) 210109. DOI:10.4491/eer.2021.109

[4]. E. le Saché, A. Alvarez Moreno, T.R. Reina, *Front. Chem*. 9 (2021) 672419. DOI: 10.3389/fchem.2021.672419

[5]. X. Cai, Y.H. Hu, *Energy Sci. Eng.* 7 (2019) 4–29. DOI: 10.1002/ese3.278

[6]. H. Zhang, Z. Sun, Y.H. Hu, *Renew. Sustain. Energy Rev.* 149 (2021) 111330. DOI: 10.1016/j.rser.2021.111330

[7]. X. Gao, J. Li, M. Zheng, S. Cai, J. Zhang, S. Askari, N. Dewangan, J. Ashok, S. Kawi, *Process Saf. Environ. Prot.* 156 (2021) 598–616. DOI: 10.1016/j.psep.2021.10.051

[8]. D. Pham Minh, X.H. Pham, T.J. Siang, D.V.N. Vo, *Appl. Catal. A Gen.* 621 (2021) 118202. DOI: 10.1016/j.apcata.2021.118202

[9]. A.S. Farooqi, M. Yusuf, N.A. Mohd Zabidi, R. Saidur, K. Sanaullah, A.S. Farooqi, A. Khan, B. Abdullah, *Int. J. Hydrogen Energy* 46 (2021) 31024–31040. DOI: 10.1016/j.ijhydene.2021.01.049

[10]. U.S. Mohanty, M. Ali, M.R. Azhar, A. Al-Yaseri, A. Keshavarz, S. Iglauer, *Int. J. Hydrogen Energy* 46 (2021) 32809–32845. DOI: 10.1016/j.ijhydene.2021.07.097

[11]. V.V. Nedolivko, G.O. Zasypalov, A.V. Vutolkina, P.A. Gushchin, V.A. Vinokurov, L.A. Kulikov, S.V. Egazar'yants, E.A. Karakhanov, A.L. Maksimov, A.P. Glotov, *Russ. J. Appl. Chem.* 93 (2020) 765–787. DOI: 10.1134/S1070427220060014

[12]. G.N. Mazo, O.A. Shlyakhtin, A.S. Loktev, A.G. Dedov, *Russ. Chem. Bull.* 68 (2019) 1949–1953. DOI: 10.1007/s11172-019-2653-6

[13]. A. Vita, L. Pino, F. Cipitì, M. Laganà, V. Recupero, *Fuel Process. Technol.* 127 (2014) 47–58. DOI: 10.1016/j.fuproc.2014.06.014

[14]. R.O. da Fonseca, A.R. Ponseggi, R.C. Rabelo-Neto, R.C.C. Simões, L.V. Mattos, F.B. Noronha, *J. CO2 Util.* 57 (2022) 101880. DOI: 10.1016/j.jcou.2021.101880

[15]. J.M. García-Vargas, J.L. Valverde, A. De Lucas-Consuegra, B. Gómez-Monedero, P. Sánchez, F. Dorado, *Appl. Catal. A Gen.* 431–432 (2012) 49–56. DOI: 10.1016/j.apcata.2012.04.016

[16]. D.M. Walker, S.L. Pettit, J.T. Wolan, J.N. Kuhn, *Appl. Catal. A Gen*. 445–446 (2012) 61–68. DOI: 10.1016/j.apcata.2012.08.015

[17]. R. Kumar, K.K. Pant, *Fuel Process. Technol.* 210 (2020) 106559. DOI: 10.1016/j.fuproc.2020.106559

[18]. C.E. Kozonoe, R.M. Brito Alves, M. Schmal, *Fuel* 281 (2020) 118749. DOI: 10.1016/j.fuel.2020.118749

[19]. A.V. Paladino Lino, C.B. Rodella, E.M. Assaf, J.M. Assaf, *Int. J. Hydrogen Energy* 45 (2020) 8418–8432. DOI: 10.1016/j.ijhydene.2020.01.002
[20]. A.J. Majewski, J. Wood, *Int. J. Hydrogen Energy* 39 (2014) 12578–12585. DOI: 10.1016/j.ijhydene.2014.06.071
[21]. J. Yoo, Y. Bang, S.J. Han, S. Park, J.H. Song, I.K. Song, *J. Mol. Catal. A Chem.* 410 (2015) 74–80. DOI: 10.1016/j.molcata.2015.09.008
[22]. I.Z. Ismagilov, E.V. Matus, V.V. Kuznetsov, S.A. Yashnik, M.A. Kerzhentsev, G. Gerritsen, H.C.L. Abbenhuis, Z.R. Ismagilov, *Eurasian Chem.-Technol. J.* 19 (2017) 3–16. DOI: 10.18321/ectj497
[23]. A.V.P. Lino, E.M. Assaf, J.M. Assaf, *Catal. Today* 289 (2017) 78–88. DOI: 10.1016/j.cattod.2016.08.022
[24]. A.G. Dedov, A.S. Loktev, V.P. Danilov, O.N. Krasnobaeva, T.A. Nosova, I.E. Mukhin, A.E. Baranchikov, K.E. Yorov, M.A. Bykov, I.I. Moiseev, *Pet. Chem.* 60 (2020) 194–203. DOI: 10.1134/S0965544120020048
[25]. E.V. Matus, D.V. Nefedova, V.V. Kuznetsov, V.A. Ushakov, O.A. Stonkus, I.Z. Ismagilov, M.A. Kerzhentsev, Z.R. Ismagilov, *Kinet. Catal.* 58 (2017) 610–621. DOI: 10.1134/S0023158417050160
[26]. C. Alvarez-Galvan, M. Melian, L. Ruiz-Matas, J.L. Eslava, R.M. Navarro, M. Ahmadi, B. Roldan Cuenya, J.L.G. Fierro, *Front. Chem*. 7 (2019). DOI: 10.3389/fchem.2019.00104
[27]. A.G. Dedov, A.S. Loktev, V.P. Danilov, O.N. Krasnobaeva, T.A. Nosova, I.E. Mukhin, A.E. Baranchikov, Kh.E. Yorov, M.A. Bykov, I.I. Moiseev, *Pet. Chem.* 59 (2019) 385–393. DOI: 10.1134/S0965544119040042
[28]. I.V. Zagaynov, A.S. Loktev, I.E. Mukhin, A.A. Konovalov, A.G. Dedov, *Mendeleev Commun*. 32 (2022) 129–131. DOI: 10.1016/j.mencom.2022.01.042
[29]. J.M. García-Vargas, J.L. Valverde, J. Díez, P. Sánchez, F. Dorado, *Appl. Catal. B Environ.* 164 (2015) 316–323. DOI: 10.1016/j.apcatb.2014.09.044
[30]. Z.A. Fedorova, M.M. Danilova, V.I. Zaikovskii, *Mater. Lett.* 261 (2020) 127087. DOI: 10.1016/j.matlet.2019.127087
[31]. L. Pino, A. Vita, M. Laganà, V. Recupero, *Appl. Catal. B Environ.* 148–149 (2014) 91–105. DOI: 10.1016/j.apcatb.2013.10.043
[32]. Z.R. Ismagilov, E.V. Matus, I.Z. Ismagilov, O.B. Sukhova, S.A. Yashnik, V.A. Ushakov, M.A. Kerzhentsev, *Catal. Today* 323 (2019) 166–182. DOI: 10.1016/j.cattod.2018.06.035
[33]. V. Fedorova, M. Simonov, K. Valeev, Y. Bespalko, E. Smal, E. Sadovskaya, T. Krieger, A. Ishchenko, V. Sadykov, N. Eremeev, *Energies* 14 (2021) 2973. DOI: 10.3390/en14102973
[34]. M.M. Danilova, Z.A. Fedorova, V.A. Kuzmin, V.I. Zaikovskii, A.V. Porsin, T.A. Krieger, *Catal. Sci. Technol.* 5 (2015) 2761–2768. DOI: 10.1039/c4cy01614a
[35]. A.F. Lucrédio, J.M. Assaf, E.M. Assaf, *Fuel Process. Technol.* 102 (2012) 124–131. DOI: 10.1016/j.fuproc.2012.04.020
[36]. I.Z. Ismagilov, E.V. Matus, D.V. Nefedova, V.V. Kuznetsov, S.A. Yashnik, M.A. Kerzhentsev, Z.R. Ismagilov, *Kinet. Catal.* 56 (2015) 394–402. DOI: 10.1134/S0023158415030064
[37]. E.V. Matus, S.D. Vasil'ev, I.Z. Ismagilov, V.A. Ushakov, M.A. Kerzhentsev, Z.R. Ismagilov, *Chem. Sustain. Dev.* 28 (2020) 403–411. DOI: 10.15372/csd2020246
[38]. U. Izquierdo, V.L. Barrio, J. Requies, J.F. Cambra, M.B. Güemez, P.L. Arias, *Int. J. Hydrogen Energy* 38 (2013) 7623–7631. DOI: 10.1016/j.ijhydene.2012.09.107
[39]. I.Z. Ismagilov, A.V. Vosmerikov, L.L. Korobitsyna, E.V. Matus, M.A. Kerzhentsev, A.A. Stepanov, E.S. Mihaylova, Z.R. Ismagilov, *Eurasian Chem.-Technol. J.* 23 (2021) 147–168. DOI: 10.18321/ectj1099
[40]. M.A. Kerzhentsev, E.V. Matus, I.A. Rundau, V.V. Kuznetsov, I.Z. Ismagilov, V.A. Ushakov, S.A. Yashnik, Z.R. Ismagilov, *Kinet. Catal.* 58 (2017) 601–622. DOI: 10.1134/S002315841705010X
[41]. Z. Ni, X. Djitcheu, X. Gao, J. Wang, H. Liu, Q. Zhang, *Sci. Rep.* 12 (2022) 5344. DOI: 10.1038/s41598-022-09291-w
[42]. N. Wang, W. Qian, W. Chu, F. Wei, *Catal. Sci. Technol.* 6 (2016) 3594–3605. DOI: 10.1039/c5cy01790d
[43]. P.G. Lustemberg, Z. Mao, A. Salcedo, B. Irigoyen, M.V. Ganduglia-Pirovano, C.T. Campbell, *ACS Catal.* 11 (2021) 10604–10613. DOI: 10.1021/acscatal.1c02154
[44]. J. Deng, W. Chu, B. Wang, W. Yang, X.S. Zhao, *Catal. Sci. Technol.* 6 (2016) 851–862. DOI: 10.1039/c5cy00893j
[45]. Y. Lyu, J. Jocz, R. Xu, E. Stavitski, C. Sievers, *ACS Catal.* 10 (2020) 11235–11252. DOI: 10.1021/acscatal.0c02426
[46]. M.A. Kerzhentsev, E.V. Matus, I.Z. Ismagilov, V.A. Ushakov, O.A. Stonkus, T.V. Larina, G.S. Kozlova, P. Bharali, Z.R. Ismagilov, *J. Struct. Chem.* 58 (2017) 133–141. DOI: 10.1134/S002247661701019X
[47]. I.Z. Ismagilov, E.V. Matus, V.V. Kuznetsov, N. Mota, R.M. Navarro, S.A. Yashnik, I.P. Prosvirin, M.A. Kerzhentsev, Z.R. Ismagilov, J.L.G. Fierro, *Appl. Catal. A Gen.* 481 (2014) 104–115. DOI:10.1016/j.apcata.2014.04.042

[48]. E.V. Matus, A.S. Shlyakhtina, O.B. Sukhova, I.Z. Ismagilov, V.A. Ushakov, S.A. Yashnik, A.P. Nikitin, P. Bharali, M.A. Kerzhentsev, Z.R. Ismagilov, *Kinet. Catal.* 60 (2019) 221–230. DOI: 10.1134/S002315841902006X

[49]. E.V. Matus, O.B. Sukhova, I.Z. Ismagilov, M.A. Kerzhentsev, L. Li, Z.R. Ismagilov, *J. Phys. Conf. Ser.* 1749 (2021) 012023. DOI: 10.1088/1742-6596/1749/1/012023

[50]. A. Löfberg, J. Guerrero-Caballero, T. Kane, A. Rubbens, L. Jalowiecki-Duhamel, *Appl. Catal. B Environ.* 212 (2017) 159–174. DOI: 10.1016/j.apcatb.2017.04.048

[51]. M.A. Kerzhentsev, E.V. Matus, I.Z. Ismagilov, O.B. Sukhova, P. Bharali, Z.R. Ismagilov, *Eurasian Chem.-Technol. J.* 20 (2018) 283–291. DOI: 10.18321/ectj761

[52]. D. Vovchok, C.J. Guild, J. Llorca, R.M. Palomino, I. Waluyo, J.A. Rodriguez, S.L. Suib, S.D. Senanayake, *Appl. Catal. A Gen.* 567 (2018) 1–11. DOI: 10.1016/j.apcata.2018.08.026

[53]. R. Murugan, G. Ravi, G. Vijayaprasath, S. Rajendran, M. Thaiyan, M. Nallappan, M. Gopalan, Y. Hayakawa, *Phys. Chem. Chem. Phys.* 19 (2017) 4396–4404. DOI: 10.1039/c6cp08281e

[54]. A. Romero-Núñez, G. Díaz, *RSC Adv.* 5 (2015) 54571–54579. DOI: 10.1039/c5ra04259c

[55]. Anushree, S. Kumar, C. Sharma, *Catal. Sci. Technol.* 6 (2016) 2101–2111. DOI: 10.1039/c5cy01083g

[56]. Z. Liu, D.C. Grinter, P.G. Lustemberg, T.D. Nguyen-Phan, Y. Zhou, S. Luo, I. Waluyo, E.J. Crumlin, D.J. Stacchiola, J. Zhou, J. Carrasco, H.F. Busnengo, M.V. Ganduglia-Pirovano, S.D. Senanayake, J.A. Rodriguez, *Angew. Chemie Int. Ed.* 55 (2016) 7455–7459. DOI: 10.1002/anie.201602489

[57]. E.V. Matus, L.B. Okhlopkova, O.B. Sukhova, I.Z. Ismagilov, M.A. Kerzhentsev, Z.R. Ismagilov, *J. Nanoparticle Res.* 21 (2019). DOI: 10.1007/s11051-018-4454-5

[58]. E.V. Matus, I.Z. Ismagilov, V.A. Ushakov, A.P. Nikitin, O.A. Stonkus, E.Y. Gerasimov, M.A. Kerzhentsev, P. Bharali, Z.R. Ismagilov, *J. Struct. Chem.* 61 (2020) 1080–1089. DOI: 10.1134/S0022476620070100

[59]. L. Wu, H.J. Wiesmann, A.R. Moodenbaugh, R.F. Klie, Y. Zhu, D.O. Welch, M. Suenaga, *Phys. Rev. B* 69 (2004) 125415. DOI: 10.1103/PhysRevB.69.125415

[60]. W.J. Jang, D.W. Jeong, J.O. Shim, H.M. Kim, H.S. Roh, I.H. Son, S.J. Lee, *Appl. Energ.* 173 (2016) 80–91. DOI: 10.1016/j.apenergy.2016.04.006

[61]. V.M. Gonzalez-DelaCruz, J.P. Holgado, R. Pereñíguez, A. Caballero, *J. Catal.* 257 (2008) 307–314. DOI: 10.1016/j.jcat.2008.05.009

[62]. A. Khaleel, Weifeng Li, K.J. Klabunde, *Nanostructured Materials* 12 (1999) 463–466. DOI: 10.1016/S0965-9773(99)00159-2

[63]. Z.R. Ismagilov, E.V. Matus, L. Li, *Phys. Usp.* (2022). DOI: 10.3367/UFNr.2021.07.039084

[64]. H.S. Roh, K.Y. Koo, W.L. Yoon, *Catal. Today* 146 (2009) 71–75. DOI: 10.1016/j.cattod.2009.01.001

[65]. P. Li, Y.H. Park, D.J. Moon, N.C. Park, Y.C. Kim, *J. Nanosci. Nanotechnol.* 16 (2016) 1562–1566. DOI: 10.1166/jnn.2016.12006

[66]. T.J. Siang, T.L.M. Pham, N. Van Cuong, P.T.T. Phuong, N.H.H. Phuc, Q.D. Truong, D.V.N. Vo, *Micropor. Mesopor. Mater.* 262 (2018) 122–132. DOI: 10.1016/j.micromeso.2017.11.028

[67]. I. Wysocka, A. Mielewczyk-Gryń, M. Łapiński, B. Cieślik, A. Rogala, *Int. J. Hydrogen Energy* 46 (2021) 3847–3864. DOI: 10.1016/j.ijhydene.2020.10.189

[68]. T. Sukonket, A. Khan, B. Saha, H. Ibrahim, S. Tantayanon, P. Kumar, R. Idem, *Energy Fuels* 25 (2011) 864–877. DOI: 10.1021/ef101479y

[69]. Z. Zhao, P. Ren, W. Li, B. Miao, *Int. J. Hydrogen Energy* 42 (2017) 6598–6609. DOI: 10.1016/j.ijhydene.2016.11.144

[70]. S. Agarwal, B.L. Mojet, L. Lefferts, A.K. Datye, Ceria, Nanoshapes-Structural and Catalytic Properties, in: Catalysis by Materials with Well-Defined Structures, 2015, pp. 31–70. DOI: 10.1016/B978-0-12-801217-8.00002-5